

## Ambient conditions disordered-ordered phase transition of two-dimensional interfacial water molecules dependent on charge dipole moment

Chunlei Wang,<sup>1,2,5,\*</sup> Chonghai Qi,<sup>1,3</sup> Yusong Tu,<sup>4</sup> Xuechuan Nie,<sup>1</sup> and Shanshan Liang<sup>1</sup>

<sup>1</sup>*Division of Interfacial Water and Key Laboratory of Interfacial Physics and Technology, Shanghai Institute of Applied Physics, Chinese Academy of Sciences, Shanghai 201800, China*

<sup>2</sup>*Shanghai Advanced Research Institute, Chinese Academy of Sciences, Shanghai 201210, China*

<sup>3</sup>*School of Physics, Shandong University, Jinan 250100, China*

<sup>4</sup>*College of Physics Science and Technology, Yangzhou University, Yangzhou 225009, China*

<sup>5</sup>*Department of Chemistry, University of Nebraska-Lincoln, Lincoln, Nebraska 68588, USA*



(Received 18 July 2018; published 3 June 2019)

Phase transitions of water molecules are commonly expected to occur only under extreme conditions, such as nanoconfinement, high pressure, or low temperature. We herein report the disordered-ordered phase transition of two-dimensional interfacial water molecules under ambient conditions using molecular-dynamics simulations. This phase transition is greatly dependent on the charge dipole moment, production of both charge values, and the dipole length of the solid surface. The phase transition can be identified by a sharp change in water-water interaction energies and the order parameters of the two-dimensional interfacial water monolayer, under a tiny dipole moment change near the critical dipole moment. The critical dipole moment of the solid material surface can classify a series of materials that can induce distinct ordered phases of surface water, which may also result in surface wetting, friction, and other properties.

DOI: [10.1103/PhysRevMaterials.3.065602](https://doi.org/10.1103/PhysRevMaterials.3.065602)

### I. INTRODUCTION

Versatile phases of water molecules with novel molecular structures that are different from the conventional bulk phases have been observed [1–20]. These multiple water phases, including a large number of ice phases and the metastable phase behavior of supercooled water, are commonly brought about by phase-transition behaviors under the extreme confinements of nanocapillaries [3–5], very high pressures [5–7], or low temperatures [9–12,21–23]. This implies that the phase transitions of water are not expected to occur under ambient conditions. Phase transitions of water under ambient conditions should be of significant importance and application because liquid water is essential for a number of physical or chemical processes [24–26], and even the biological functions [27–30]. Some crystal solid surfaces, such as ionic crystals or clays (such as NaCl [2] or talc [31,32]), can feature highly polarizable atoms with charge or charge dipoles. When the polarizable water molecules adhere to the surfaces due to strong charge-dipole or dipole-dipole interactions, they may arrange themselves to form a hydrogen-bonded network that yields to the surface atomic structures [33–41]. However, at ambient conditions, thermal fluctuations often break the hydrogen-bonded networks. This can make it difficult to observe the phase transitions of liquid water under ambient conditions, even though observations of ordered water on certain solid surfaces, such as mica, have been reported [39–41].

In this paper, we present the disordered-ordered phase transitions of a two-dimensional interfacial water monolayer, under ambient conditions, that are greatly dependent on a reaction coordinate, namely, the charge dipole moment of the solid surface. We have found the critical dipole moment of the solid material surface that can classify a series of materials with distinct ordered phases of surface water. The phase transition can be identified by the sharp changes in the water-water interaction energies of the two-dimensional interfacial water monolayer and the order parameters of the water dipole orientation, under a very tiny change ( $< 1 D$ ) near the critical dipole moment. We have also plotted the phase diagram of the wetting behavior on the charge dipoles. The physics of the transition are attributed to the charge dipole length on the surface that can accommodate the stable hydrogen-bonded network of the water monolayer. The ordered phase transitions of a two-dimensional interfacial water monolayer induces a wetting phenomenon, termed “ordered water that does not completely wet water” on a superhydrophilic surface, consistent with our previous works [42–45].

### II. SIMULATION METHODS

The molecular-dynamics (MD) simulation has been widely used to study the phase behaviors of water systems [46–49]. We here performed the MD simulations employing the GROMACS 4.5.4 package [50] in the canonical (NVT) ensemble, where the number of particles ( $N$ ), the simulations box volume ( $V$ ), and the temperature ( $T$ ) were kept constant. The temperature was fixed at  $T = 300$  K by using a Berendsen thermostat. In the simulations, the planar hexagonal structure

\*wangchunlei@sinap.ac.cn

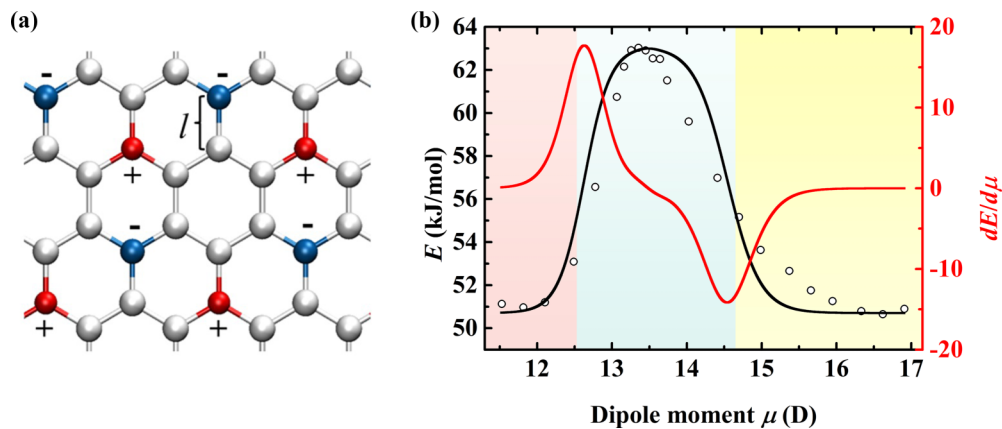


FIG. 1. (a) Geometry of the solid surface model. The red and blue spheres represent the atoms of the solid with positive and negative charges, respectively, while the silver spheres represent neutral solid atoms. (b) Plot of absolute values of attractive interaction energy values  $E$  of one water molecule in the first water monolayer and its neighboring water molecules in the same monolayer, versus the solid surface dipole moment  $\mu$  for the system with a 4-nm-thick water film, together with the differentiated values  $dE/d\mu$  (right red axis).

of the solid surfaces was composed of 1664 solid atoms [see Fig. 1(a)] parallel to the  $x$ - $y$  plane, similar as our previous work [43]. All the directions of the simulation systems were set for periodicity. We chose the rigid extended simple point-charge (SPC/E) water model [51] as the explicit solvent. The nearest-neighbor bond length (denoted  $l$ ) was set to increase from 0.120 to 0.176 nm in intervals of 0.03 or 0.04 nm. Specifically, for  $l = 0.136$  to 0.143 nm, the interval was 0.01 nm. The surface dimensions ranged from  $5.40 \times 5.76 \text{ nm}^2$  to  $7.93 \times 8.45 \text{ nm}^2$  and the box sizes in the  $z$  axis of all the systems are set as 25.0 nm. For these types of surfaces, the positive and negative charges of the same quantity  $q$  fell in  $[0.5e, 1.0e]$  with the interval of  $0.1e$  assigned to the atoms that were located diagonally in neighboring hexagons [42–45] [see Fig. 1(a)]. Overall, the model solid surface was neutral. For these solid surfaces, we have performed two series of systems (see Fig. S10 in Supplemental Material (SM) [52]) To analyze the water density distribution and water-water interaction and the order parameter, we performed simulations for systems with a 4-nm-thick water film with the number of water molecules increasing from 3525 to 6521 for various sizes of the systems. To compute the water contact angle, the systems contained water molecules with the number of water molecules ranging from 530 to 1043 for various sizes of the systems. For all the systems, the simulation time was 100 ns, and the data in the last 20 ns were collected for analysis. The time step was 1 fs. The Lennard-Jones (LJ) parameters of the solid atoms were  $\epsilon_{ss} = 0.439 \text{ kJ/mol}$  and  $\sigma_{ss} = 3.343 \text{ \AA}$  [43]. The Lorentz-Berthelot combining rules for water molecules and the substrate were used, with the form  $\epsilon_{ij} = (\epsilon_{ii} \times \epsilon_{jj})^{1/2}$  and  $\sigma_{ij} = (\sigma_{ii} + \sigma_{jj})/2$ , where  $\epsilon_{ii}$  and  $\sigma_{ii}$  were the parameters of atom  $i$  for the LJ diameter and well depth, respectively. The LJ parameters between O atoms in water molecules and substrate atoms were  $\sigma_{S-O} = 3.255 \text{ \AA}$  and  $\epsilon_{S-O} = 0.535 \text{ kJ/mol}$ . The particle-mesh Ewald method with a correction term of slab geometry [53] and a real-space cutoff of  $10 \text{ \AA}$  were used to treat long-range electrostatic interactions, and  $10\text{-\AA}$  cutoff was applied to all van der Waals interactions. In addition, the criterion for the hydrogen bond between water molecules was that, simultaneously, the O-O

distance was less than  $3.5 \text{ \AA}$  and the angle H-O...O was less than  $30^\circ$ .

### III. RESULTS AND DISCUSSION

The first water layer [9,42–45,54] is usually the key to understanding various surface properties. For the first series of systems studied, with a water thickness of 4 nm, we focus on the absolute values of the attraction interaction energy  $E$  (sum of the LJ interaction and electrostatic interaction) of one water molecule in the first water monolayer with its neighboring molecules in the same monolayer in terms of the surface charge dipoles  $\mu$  (more details can be found in PS 5 and PS 6 in SM). The results are shown in Fig. 1(b). Here, the water molecules adopted are in the first water layer, with a thickness of 0.4 nm (see also the density profiles of water near the solid surfaces in Fig. S1 in SM) [42,43], and the dipole moment is calculated using  $\mu = qL$  (where  $L = 2l$  is the dipole length,  $l$  is the bond length, and  $q$  is the charge setting as  $1.0e$ ). The interaction  $E$  versus dipole moment  $\mu$  exhibits a two-step character (separated by three regions with different colors) that can be fitted piecewise using the tanh function. The differentiated values of the fitted energy with respect to the dipole moment (i.e.,  $dE/d\mu$ ) exhibit three flat regions. As  $\mu$  increases from 11.5 to 13.5 D, the potential energy is first constant and then suddenly increases by 12 kJ/mol by a small dipole moment change (1.0 D). This large energy change is almost twice that of the 5.6-kJ/mol energy drop observed during the first-order phase transition confined between two parallel walls [1], and is larger than the 7.0 kJ/mol at the freezing transition of bulk water obtained using a 4-point transferable intermolecular potential TIP4P water model [55]. The relatively sharp changes in energy suggest a strong phase transition for the first two-dimensional water layer. As  $\mu$  increases from 13.5 to 17.0 D, the potential energy suddenly decreases by about 12 kJ/mol. Such relatively sharp changes in energy again suggest a strong phase transition for the first two-dimensional water layer. These results show a clear two-step phase transition as the charge dipole moment increases,

which was not well understood in our previous studies [42–45]. We emphasize that the phase transition is found to be dependent on the charge dipole moment of the solid surface, and is observed under ambient conditions, with no need for extreme nanoconfinement, high pressure, or low temperature. More importantly, similar phase-transition dependence on the lattice constant of the nonpolar face-centered-crystal (fcc) solid surface is observed under ambient conditions (see PS 2 of SM), indicating the generality of this observation. The atomic distance of the fcc(100) surface inducing the ordered water structures falls in the region 0.26 to 0.30 nm, which is exactly as the dipole length region (0.26 to 0.30 nm) of our hexagonal lattice structures.

To further characterize the phase transitions of the water structures, we calculate the probability distribution of the water dipole orientation angle  $\varphi$ , which is the angle between the projection of a water molecule dipole orientation onto the  $xy$  plane and a crystallographic direction (see three typical examples in Fig. S4 in SM) [42,43]. Accordingly, we calculated the fluctuations of the probability (denoted as  $S$ ) of the water monolayer dipole orientation angle  $\varphi$  to measure the degree of ordered water:

$$S = \sqrt{\frac{1}{N} \sum_{i=1}^N (p_i - \langle p \rangle)^2}, \quad (1)$$

where  $N = 72$  is the total number of intervals,  $p_i$  represents the probability of the water dipole orientation angle  $\varphi$  falling in the  $i$ th interval, and  $\langle p \rangle$  are the average values of the probability. Then, we can define the order parameter  $\eta$  as

$$\eta = S/S_{\max}, \quad (2)$$

where  $S_{\max}$  is determined by the probability distribution of the water monolayer outside the droplet for 13.4 D ( $l = 0.14$  nm), which can be regarded as the most ordered water structure. The results of the order parameters versus the charge dipole moment are shown in Fig. 2. We can clearly see that the order parameters are very small (0.1) when the dipole moment is as small as 11.5 D. As the dipole moment increases, the order parameter  $\eta$  first increases and then decreases, and the maximum value (0.52) is locating at 13.3 D. The sharp change in the order parameter suggests that this is a disordered-ordered phase transition of a two-dimensional water monolayer that is dependent on the solid surface dipole moment (see three typical snapshots of water molecular structures in Fig. 2). We have also found that the ordered water is induced within a critical dipole moment range from 12.5 to 14.4 D, corresponding to the change in the charge dipole length from 0.26 to 0.30 nm at a fixed charge value  $1.0 e$ . As discussed in PS 4 in SM, the temperature can also induce the similar disordered-ordered phase transition of a two-dimensional water monolayer.

The microscopic mechanism of the phase transition from disordered to ordered water monolayer is attributed to the hydrogen-bonds network of the first water monolayer. We have computed the average number of hydrogen bonds formed by a water molecule in the monolayer with its neighboring water molecules in the same layer. As shown in Fig. 3, the hydrogen bond number first increases, and then remains constant, while it then decreases again, as the surface charge dipole moment increases. The more hydrogen bonds formed

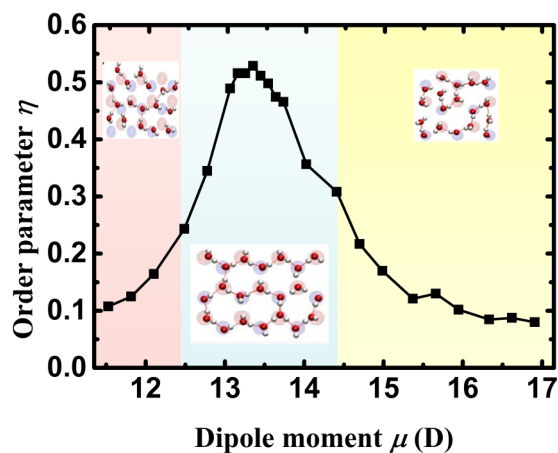


FIG. 2. Order parameter  $\eta$  derived from the probability distribution of the water dipole orientation angle in the first water monolayer versus the charge dipole moment  $\mu$  for the system with a 4-nm-thick water film. The three typical snapshots show the disordered or ordered water structures of the first monolayer. The red lines represent the hydrogen bonds between the water molecules. Inset snapshots of the water monolayer on the charged solid surfaces are shown with the positions of the positive (light red) and negative (light blue) charges.

within the water monolayer, the larger the absolute values of the water-water interactions. This relationship is consistent with the order parameters of the first water monolayer (see Fig. 2) and is dependent on the surface charge dipole moments. Due to the more hydrogen bonds formation when ordered water formed, the exchange behavior of the ordered first water to the other layers becomes much more rare than the disordered first water. As shown in Fig. S8 in SM, the exchange rate is  $0.058 \text{ ps}^{-1}$  for an ordered water monolayer formed on the solid surface with  $\mu = 13.6 \text{ D}$  ( $l = 0.142 \text{ nm}$ ), which is much smaller comparing with  $14.505 \text{ ps}^{-1}$  for disordered water monolayer with  $\mu = 11.5 \text{ D}$  ( $l = 0.120 \text{ nm}$ ) and  $3.722 \text{ ps}^{-1}$  for disordered water monolayer with  $\mu = 16.3 \text{ D}$  ( $l = 0.170 \text{ nm}$ ). Correspondingly, the dwell time of

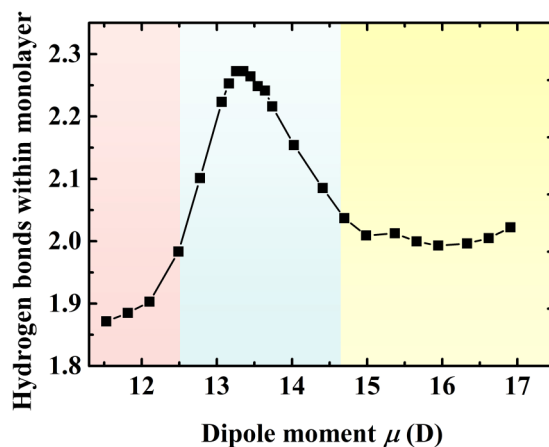


FIG. 3. Number of hydrogen bonds that one water molecule in the water monolayer can form between the water monolayer for various charge dipole moments.

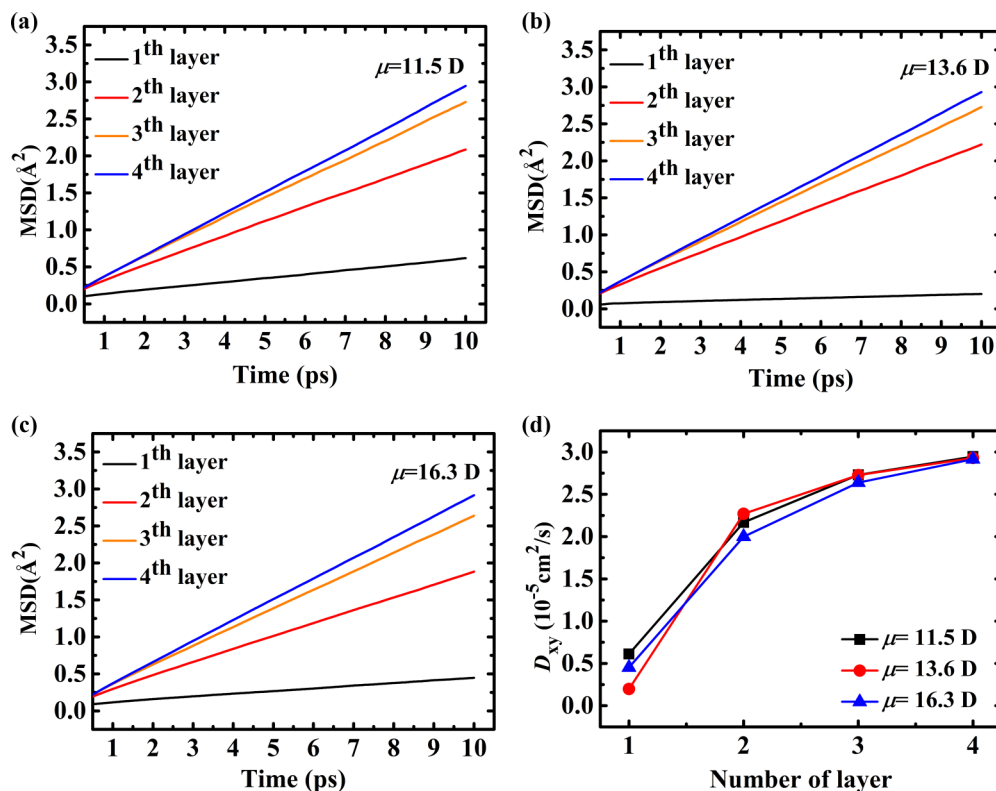


FIG. 4. (a)–(c) Mean-square displacement of the water molecules in various layers that are in parallel of the surface for  $\mu = 11.5, 13.6,$  and  $16.3$  D, respectively. (d) In-plane self-diffusion coefficient ( $D_{xy}$ ) of water molecules in various layers.

the ordered first water layer is over one order of magnitude larger than the other two disordered first water layers (see Fig. S9 in SM).

The dynamics properties of the interfacial water, e.g., mean-square displacement (MSD), of water molecules in  $xy$  plane for various water layers are calculated. Here, we choose the water layer according to the distance of water molecules to the solid surfaces:  $0 \text{ \AA} < z_{\text{layer}1} \leq 4 \text{ \AA}$  as the first layer,  $4 \text{ \AA} < z_{\text{layer}2} \leq 7.5 \text{ \AA}$  as the second layer,  $7.5 \text{ \AA} < z_{\text{layer}3} \leq 11 \text{ \AA}$  as the third layer, and  $11 \text{ \AA} < z_{\text{layer}4} \leq 15 \text{ \AA}$  as the fourth layer. Three typical systems with various dipole moments dipole moment  $\mu = 11.5, 13.6,$  and  $16.3$  D that correspond to the dipole length  $l = 0.120, 0.142,$  and  $0.170$  nm, respectively, are chosen and the results are shown in Figs. 4(a)–4(c). One can observe that there is a clear linear relationship between the water mean-square displacement and the time  $t$ . As the water molecule approaches the solid surfaces, the MSD of water molecules becomes smaller. Accordingly, we can obtain the self-diffusion coefficient  $D_{xy}$  of water molecule by measuring MSD of water molecules for various water layers for systems with different solid surfaces. As shown in Fig. 4(d), the self-diffusion coefficient gradually increases as the water molecule is far away from the solid surface. We have found the interesting phenomenon for the diffusion constant  $D_{xy}$  of the first and second water layers on the various solid surfaces. As for the first water layer, the  $D_{xy}$  values for various surfaces with different charge dipoles are  $0.595 \times 10^{-5} \text{ cm}^2/\text{s}$ ,  $0.207 \times 10^{-5} \text{ cm}^2/\text{s}$ , and  $0.436 \times 10^{-5} \text{ cm}^2/\text{s}$  for  $\mu = 11.5, 13.6,$  and  $16.3$  D, respectively.

Clearly, the diffusion constant of the ordered water phase is less than one half of the other two disordered water phases. These two self-diffusion values are much smaller than the bulk water self-diffusion value of  $2.95 \times 10^{-5} \text{ cm}^2/\text{s}$ . However, to our surprise, the self-diffusion constant for the second water layer ( $4 \text{ \AA} < z_{\text{layer}2} \leq 7.5 \text{ \AA}$ ) near ordered water is  $2.157 \times 10^{-5} \text{ cm}^2/\text{s}$ , which is obviously larger than  $2.009 \times 10^{-5} \text{ cm}^2/\text{s}$  and  $1.809 \times 10^{-5} \text{ cm}^2/\text{s}$  of the other two solid surfaces, quite consistent with our previous work [56]. This can be attributed to the distinct phases of the first water layer that can induce the redistribution of the number of hydrogen bonds formed per water molecule in the first layer. We find that the hydrogen bonds number per water molecule formed between the neighbor water molecules is 2.24 for the surface charge dipole  $13.6$  D with  $l = 0.142$  nm, which is more than 1.99 for the previous surface with  $16.3$  D with  $l = 0.170$  nm and 1.87 for the surface with  $11.5$  D with  $l = 0.120$  nm (see Fig. 3). This thus induces the fewer number of hydrogen bonds formed between the ordered water and water molecule and the decrease of the attraction energy between each water molecule in the water monolayer and the water molecules above. This makes water molecules diffuse more easily near the ordered water monolayer, consistent with our previous work [56].

Why does such a disordered-ordered transition occur? The physics of the transition depends on whether the charge dipole moment can accommodate the hydrogen-bonded network of the water monolayer. First, to understand this critical dipole length, we have chosen typical configurations for the water

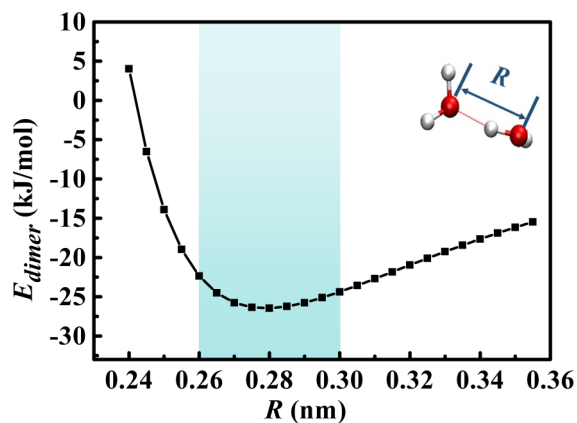


FIG. 5. Interaction energy  $E_{\text{dimer}}$  between the water dimers versus oxygen-oxygen distance,  $R$ . The light blue area corresponds to the critical dipole moment between 12.5 and 14.4 D, with the dipole length between 0.26 and 0.30 nm.

dimer (see upper inset in Fig. 5) in the first water monolayer, and adjusted the oxygen-oxygen distance  $R$  between the water dimer. Here, we assume that this dimer configuration does not change, and that one of its water molecules is bound by the surface positive charge, while the other is bound by the negative charge, during the variation of  $R$ . We then calculate the interactions,  $E_{\text{dimer}}$ , between the water dimers with respect to  $R$ , which could reflect the intensity of the hydrogen bonds between the water molecules. As shown in Fig 5, the  $E_{\text{dimer}}$  values are dependent on  $R$ . In the critical distance, between  $R = 0.26$  nm and  $R = 0.30$  nm (light blue area), the intensity of the hydrogen bonds formed between the dimer water molecules approaches a valley value ( $-26.5$  kJ/mol), which just falls within the region of the critical dipole length corresponding to the ordered water (see Fig. 5). This critical distance facilitates the water molecules in the first layer to form hydrogen bonds with the same monolayer (see also Fig. 3), which stabilizes the ordered hydrogen-bond network between the water molecules in the monolayer. Moreover, the charge dipole length of the solid surfaces is extremely important for accommodating the hydrogen-bonded network of the water monolayer. We have found that the ordered water monolayer can be found only in the critical region of the charge dipole length (see Fig. 2).

In addition, the hexagonal solid surfaces are the structural basis of the hexagonal water hydrogen-bonded network. As we know, the H–O–H bond angle of the water molecule is  $109.5^\circ$ , which is close to the  $120^\circ$  theoretical value for three bonded atoms. This water molecular structure favors the matching between water molecules and solid surfaces. Each water molecule can form three hydrogen bonds with three neighboring water molecules (see the middle snapshot in Fig. 2). Simultaneously, the water molecules have the oxygen atoms pointing to the surface of positive charges and the hydrogen atoms pointing to the negative charge on the surfaces (see also snapshot in Fig. S3 of SM). This can occupy one potential hydrogen-bonding donor or acceptor position [42,43]. This requires relatively large charge values ( $q > 0.5e$ ) of the solid surface atoms that arise from the stable electrostatic adsorption of the water molecules.

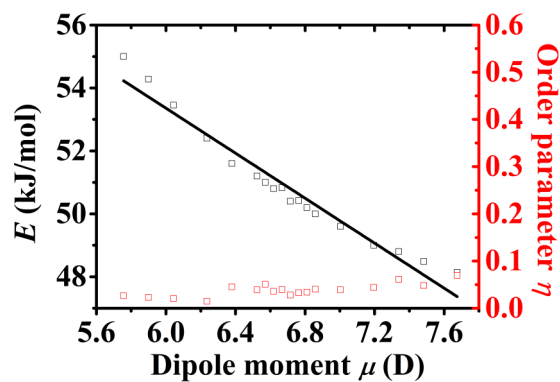


FIG. 6. Absolute values of attractive interaction energy values  $E$  of one water molecule in the first water monolayer with its neighboring water molecules in the same monolayer (left black axis) and the order parameter  $\eta$  (right red axis), versus the solid surface dipole moment  $\mu$  for the systems with 4-nm-thick water film when  $q = 0.5e$ .

Consequently, this ordered water structure favors four saturated hydrogen bonds for each water molecule for the formation of a hydrogen-bonded network between the water molecules at the solid surfaces.

The observed complex phase-transition behaviors require necessarily relatively large charge values. As shown in Fig. 6, for  $q = 0.5e$  the absolute values of water-water attractive interaction values  $E$  decrease linearly with the increase in dipole moment and the order parameters  $\eta$  are always very small at around 0.05 without any sharp changes. It should be noted that the water-water attractive interaction values  $E$  for  $q = 0.5e$  are at least 5 kJ/mol weaker than the peak values of that for  $q = 1.0e$ , and the order parameter  $\eta$  is about one order of magnitude smaller than the peak values of that for  $q = 1.0e$ . Clearly, these results show that there is no disordered-ordered phase transition in the water molecules of the monolayer for the charge  $q = 0.5e$ . As for the wetting behavior, the solid surfaces are completely wetted with the water film spreading all over the surfaces for all dipole lengths at a fixed  $q = 0.5e$ , as shown in Fig. 7. This can be attributed to the weak charges that are not strong enough to enforce the

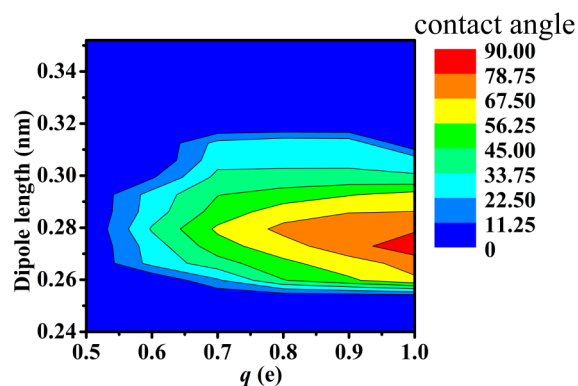


FIG. 7. Contours of the contact angles of the water droplets on the solid surfaces with the different charge values  $q$  and bond length  $l$ .

formation of ordered water structures, even though the dipole length is appropriate.

To present the phase diagram of the wetting phenomenon on the charge dipole moment  $\mu$ , we have plotted in Fig. 7 the contact angles that are dependent on the charge and dipole length. As the charge  $q$  changes from 0.6 to 1.0  $e$ , the wetting behaviors become quite complex. Briefly, there is a dipole length region with the molecular-scale hydrophilicity phenomenon that an “ordered water monolayer that does not completely wet water” [42–44,54]. For the charge  $q = 0.6 e$ , the dipole length lies in the range 0.266–0.30 nm in the case of the emergence of the water droplet. This region becomes broader with the range 0.260–0.312 nm for  $q = 0.8 e$ . Similar to the ordered-disordered phase transitions observed in Fig. 1(b), clear wetting transitions occur as the dipole moment increases. For the region  $12.5 D < \mu < 14.6 D$  as  $q = 1.0 e$ , the partially wetted is observed at room temperature, corresponding to the larger water-water attractive interaction  $E$ . Note that the contact angle can be as high as  $80^\circ$  for  $\mu = 13.0 D$ . As the charge dipole moment further increases, i.e.,  $\mu > 14.6 D$ , the water-water interaction  $E$  decreases and the surface is completely wetted again, consistent with our previous work [42–45].

#### IV. CONCLUSIONS

In contrast to the extreme conditions that induce the phase transition of water molecules, a disordered-ordered phase transition is observed to occur under ambient conditions. This phase transition is dependent on a reaction coordinate, the charge dipole moment of the solid surface. The critical

dipole moment of the solid material surface can classify series of materials with distinct ordered phases of surface water. The complex phase behaviors of water molecules will greatly affect other surface properties such as surface wetting [42–44,54], surface friction [44], surface thermal conduction [57], molecular adsorption [58,59], and even biological functions [2]. For example, the formation of ordered water can induce a particular surface-wetting phenomenon, termed ordered water monolayer that does not completely wet water, under ambient conditions [31,60–63]. These results in turn show that such disordered-ordered phase transitions in two-dimensional interfacial water molecules even under ambient conditions can be experimentally observed on such solid surfaces by adjusting the lattice constants of the real materials surfaces to match the hydrogen bonds of water molecules.

#### ACKNOWLEDGMENTS

We gratefully acknowledge Prof. Haiping Fang, Prof. Xiaocheng Zeng, Prof. Guosheng Shi, and Dr. Nan Sheng for their helpful discussions. This study was supported by the National Natural Science Foundation of China (Grants No. 11674345, No. 11675138, and No. U1532260), Key Research Program of Chinese Academy of Sciences (Grant No. QYZDJ-SSW-SLH019), Youth Innovation Promotion Association CAS (Grant No. 2014233), the Deepcomp7000 and ScGrid of the Supercomputing Center, the Computer Network Information Center of the Chinese Academy of Sciences, the Special Program for Applied Research on SuperComputation of the NSFC-Guangdong Joint Fund (second phase), and the Shanghai Supercomputer Center of China.

- 
- [1] K. Koga, H. Tanaka, and X.C. Zeng, *Nature (London)* **408**, 564 (2000).
- [2] J. Peng, D. Cao, Z. He, J. Guo, P. Hapala, R. Ma, B. Cheng, J. Chen, W. J. Xie, X.-Z. Li, P. Jelínek, L.-M. Xu, Y. Q. Gao, E.-G. Wang, and Y. Jiang, *Nature (London)* **557**, 701 (2018).
- [3] K. Koga, X. C. Zeng, and H. Tanaka, *Phys. Rev. Lett.* **79**, 5262 (1997).
- [4] G. Algara-Siller, O. Lehtinen, F. C. Wang, R. R. Nair, U. Kaiser, H. A. Wu, A. K. Geim, and I. V. Grigorieva, *Nature (London)* **519**, 443 (2015).
- [5] Y. Zhu, F. Wang, J. Bai, X. C. Zeng, and H. Wu, *ACS Nano* **9**, 12197 (2015).
- [6] N. Giovambattista, P. J. Rossky, and P. G. Debenedetti, *Phys. Rev. Lett.* **102**, 050603 (2009).
- [7] J. Bai and X. C. Zeng, *Proc. Natl. Acad. Sci. USA* **109**, 21240 (2012).
- [8] V. Rozsa, D. Pan, F. Giberti, and G. Galli, *Proc. Natl. Acad. Sci. USA* **115**, 6952 (2018).
- [9] K. Liu, C. Wang, J. Ma, G. Shi, X. Yao, H. Fang, Y. Song, and J. Wang, *Proc. Natl. Acad. Sci. USA* **113**, 14739 (2016).
- [10] M. Fitzner, G. C. Sosso, S. J. Cox, and A. Michaelides, *J. Am. Chem. Soc.* **137**, 13658 (2015).
- [11] L. Xu, P. Kumar, S. V. Buldyrev, S.-H. Chen, P. H. Poole, F. Sciortino, and H. E. Stanley, *Proc. Natl. Acad. Sci. USA* **102**, 16558 (2005).
- [12] S. Woutersen, B. Ensing, M. Hilbers, Z. Zhao, and C. A. Angell, *Science* **359**, 1127 (2018).
- [13] S. H. Han, M. Y. Choi, P. Kumar, and H. E. Stanley, *Nat. Phys.* **6**, 685 (2010).
- [14] J. Bai, C. A. Angell, and X. C. Zeng, *Proc. Natl. Acad. Sci. USA* **107**, 5718 (2010).
- [15] J. Duboisset and P.-F. Brevet, *Phys. Rev. Lett.* **120**, 263001 (2018).
- [16] Y. He, K.-i. Nomura, R. K. Kalia, A. Nakano, and P. Vashishta, *Phys. Rev. Mater.* **2**, 115605 (2018).
- [17] Z. Ding, L. Yan, Z. Li, W. Ma, G. Lu, and S. Meng, *Phys. Rev. Mater.* **1**, 045404 (2017).
- [18] F. Mei, X. Zhou, J. Kou, F. Wu, C. Wang, and H. Lu, *J. Chem. Phys.* **142**, 134704 (2015).
- [19] J. Liu, C. Zhu, K. Liu, Y. Jiang, Y. Song, J. S. Francisco, X. C. Zeng, and J. Wang, *Proc. Natl. Acad. Sci. USA* **114**, 11285 (2017).
- [20] E. B. Moore and V. Molinero, *Nature (London)* **479**, 506 (2011).
- [21] A. Haji-Akbari and P. G. Debenedetti, *Proc. Natl. Acad. Sci. USA* **112**, 10582 (2015).
- [22] Y. Xu, N. G. Petrik, R. S. Smith, B. D. Kay, and G. A. Kimmel, *J. Phys. Chem. Lett.* **8**, 5736 (2017).
- [23] F. Martelli, N. Giovambattista, S. Torquato, and R. Car, *Phys. Rev. Mater.* **2**, 075601 (2018).
- [24] B. J. Berne, J. D. Weeks, and R. H. Zhou, *Annu. Rev. Phys. Chem.* **60**, 85 (2009).
- [25] C. Zhu, H. Li, Y. Huang, X. C. Zeng, and S. Meng, *Phys. Rev. Lett.* **110**, 126101 (2013).

- [26] A. Schlaich, J. Kappler, and R. R. Netz, *Nano Lett.* **17**, 5969 (2017).
- [27] P. Ball, *Proc. Natl. Acad. Sci. USA* **114**, 13327 (2017).
- [28] P. Ball, *Chem. Rev.* **108**, 74 (2008).
- [29] R. H. Zhou, X. H. Huang, C. J. Margulis, and B. J. Berne, *Science* **305**, 1605 (2004).
- [30] H. G. Kalashami, M. Neek-Amal, and F. M. Peeters, *Phys. Rev. Mater.* **2**, 074004 (2018).
- [31] B. Rotenberg, A. J. Patel, and D. Chandler, *J. Am. Chem. Soc.* **133**, 20521 (2011).
- [32] J. W. Wang, A. G. Kalinichev, and R. J. Kirkpatrick, *Geochim. Cosmochim. Acta* **70**, 562 (2006).
- [33] S. A. Zielke, A. K. Bertram, and G. N. Patey, *J. Phys. Chem. B* **119**, 9049 (2015).
- [34] N. Giovambattista, P. G. Debenedetti, and P. J. Rossky, *J. Phys. Chem. B* **111**, 9581 (2007).
- [35] G. A. Kimmel, M. Baer, N. G. Petrik, J. VandeVondele, R. Rousseau, and C. J. Mundy, *J. Phys. Chem. Lett.* **3**, 778 (2012).
- [36] A. Verdaguer, G. M. Sacha, H. Bluhm, and M. Salmeron, *Chem. Rev.* **106**, 1478 (2006).
- [37] O. Björneholm, M. H. Hansen, A. Hodgson, L.-M. Liu, D. T. Limmer, A. Michaelides, P. Pedevilla, J. Rossmeisl, H. Shen, G. Tocci, E. Tyrode, M.-M. Walz, J. Werner, and H. Bluhm, *Chem. Rev.* **116**, 7698 (2016).
- [38] P. Guo, Y. S. Tu, J. R. Yang, C. L. Wang, N. Sheng, and H. P. Fang, *Phys. Rev. Lett.* **115**, 186101 (2015).
- [39] J. Hu, X. D. Xiao, D. F. Ogletree, and M. Salmeron, *Science* **268**, 267 (1995).
- [40] M. Odelius, M. Bernasconi, and M. Parrinello, *Phys. Rev. Lett.* **78**, 2855 (1997).
- [41] K. Xu, P. G. Cao, and J. R. Heath, *Science* **329**, 1188 (2010).
- [42] C. Wang, B. Zhou, P. Xiu, and H. Fang, *J. Phys. Chem. C* **115**, 3018 (2011).
- [43] C. Wang, H. Lu, Z. Wang, P. Xiu, B. Zhou, G. Zuo, R. Wan, J. Hu, and H. Fang, *Phys. Rev. Lett.* **103**, 137801 (2009).
- [44] C. Wang, B. Wen, Y. Tu, R. Wan, and H. Fang, *J. Phys. Chem. C* **119**, 11679 (2015).
- [45] C. Qi, B. Zhou, C. Wang, Y. Zheng, and H. Fang, *Phys. Chem. Chem. Phys.* **19**, 6665 (2017).
- [46] Y. Tu, L. Zhao, and H. Fang, *Sci. China-Phys. Mech. Astron.* **59**, 110511 (2016).
- [47] G. Menzl, J. Köfinger, and C. Dellago, *Phys. Rev. Lett.* **109**, 020602 (2012).
- [48] W. F. Kuhs, T. C. Hansen, and A. Falenty, *J. Phys. Chem. Lett.* **9**, 3194 (2018).
- [49] L. Zhao, C. Wang, J. Liu, B. Wen, Y. Tu, Z. Wang, and H. Fang, *Phys. Rev. Lett.* **112**, 078301 (2014).
- [50] B. Hess, C. Kutzner, D. van der Spoel, and E. Lindahl, *J. Chem. Theory Comput.* **4**, 435 (2008).
- [51] H. J. C. Berendsen, J. R. Grigera, and T. P. Straatsma, *J. Phys. Chem.* **91**, 6269 (1987).
- [52] See Supplemental Material at <http://link.aps.org/supplemental/10.1103/PhysRevMaterials.3.065602> for density of water layer, dipole orientation of the water monolayer, effect of the temperature on the ordered water monolayer, details of the surface-water interactions and water-water interactions of the first water monolayer, effect of the simulation box on the water-water interactions in the first water monolayer, and the order parameters, exchange behaviors, and residence time of water molecules of the adjacent water layer, and simulation size of the simulation box.
- [53] I.-C. Yeh and M. L. Berkowitz, *J. Chem. Phys.* **111**, 3155 (1999).
- [54] C. Wang, Y. Yang, and H. Fang, *Sci. China-Phys. Mech. Astron.* **57**, 802 (2014).
- [55] G. T. Gao, X. C. Zeng, and H. Tanaka, *J. Chem. Phys.* **112**, 8534 (2000).
- [56] X. Yu, C. Qi, and C. Wang, *Chin. Phys. B* **27**, 060101 (2018).
- [57] J. Cheh, Y. Gao, C. Wang, H. Zhao, and H. Fang, *J. Stat. Mech.* (2013) P06009.
- [58] X. Nie, B. Zhou, C. Wang, and H. Fang, *Nucl. Sci. Technol.* **29**, 18 (2018).
- [59] X. Nie, J. Chen, N. Sheng, L. Zeng, H. Yang, and C. Wang, *Mol. Simul.* **43**, 1377 (2017).
- [60] J. Lutzenkirchen, R. Zimmermann, T. Preocanin, A. Filby, T. Kupcik, D. Kuttner, A. Abdelmonem, D. Schild, T. Rabung, M. Plaschke, F. Brandenstein, C. Werner, and H. Geckeis, *Adv. Colloid Interface Sci.* **157**, 61 (2010).
- [61] A. Phan, T. A. Ho, D. R. Cole, and A. Striolo, *J. Phys. Chem. C* **116**, 15962 (2012).
- [62] D. T. Limmer, A. P. Willard, P. Madden, and D. Chandler, *Proc. Natl. Acad. Sci. USA* **110**, 4200 (2013).
- [63] Z. Xu, Y. Gao, C. L. Wang, and H. P. Fang, *J. Phys. Chem. C* **119**, 20409 (2015).